Structure, Vol. 10, 311–317, March, 2002, ©2002 Elsevier Science Ltd. All rights reserved. PII S0969-2126(02)00699-8

Structure and Dynamics of the Anticodon Arm Binding Domain of *Bacillus stearothermophilus* Tyrosyl-tRNA Synthetase

J. Iñaki Guijarro,[1,5] Alessandro Pintar,[1,5,6] Ada Prochnicka-Chalufour,[1,5] Valérie Guez,[2] Bernard Gilquin,[3] Hugues Bedouelle,[2,4] and Muriel Delepierre[1,4]

[1] Unité de RMN des Biomolécules and
[2] Unité de Biochimie Cellulaire
CNRS URA 2185
Institut Pasteur
28 rue du Docteur Roux
75724 Paris Cedex 15
France

[3] CEA Saclay DSV DIEP
Bâtiment 152
91191 Gif sur Yvette Cedex
France

Summary

The structure of a recombinant protein, TyrRS(Δ4), corresponding to the anticodon arm binding domain of *Bacillus stearothermophilus* tyrosyl-tRNA synthetase, has been solved, and its dynamics have been studied by nuclear magnetic resonance (NMR). It is the first structure described for such a domain of a tyrosyl-tRNA synthetase. It consists of a five-stranded β sheet, packed against two α helices on one side and one α helix on the other side. A large part of the domain is structurally similar to other functionally unrelated RNA binding proteins. The basic residues known to be essential for tRNA binding and charging are exposed to the solvent on the same face of the molecule. The structure of TyrRS(Δ4), together with previous mutagenesis data, allows one to delineate the region of interaction with $tRNA^{Tyr}$.

Introduction

Aminoacyl-tRNA synthetases are the enzymes that translate the genetic code in vivo. Each synthetase specifically links an amino acid to its anticodons through the charging of the cognate tRNAs. The amino acid is first activated with ATP to form an aminoacyl-adenylate and then transferred from this intermediate to the acceptor end of the tRNA [1]. The synthetases are modular proteins. In addition to their catalytic domain, whose fold is conserved and belongs to one of two classes, most synthetases possess one or two idiosyncratic domains [2]. These latter domains specifically recognize the anticodon arm of the cognate tRNA and are of utmost importance for the accuracy of charging.

Tyrosyl-tRNA synthetase (TyrRS) is a homodimeric protein that catalyses the formation of tyrosyl-$tRNA^{Tyr}$. The crystal structure of TyrRS from *Bacillus stearothermophilus* has been solved at 2.3 Å resolution [3]. Each monomer comprises three domains: (1) the catalytic α/β domain (residues 1–247), which contains the binding sites for tyrosine, the tyrosyl-adenylate intermediate, the acceptor stem of $tRNA^{Tyr}$, and the dimerization interface; (2) the α-helical domain (248–319), with a catalytic loop at one end and at the other end residue F_{323}, which interacts with $tRNA^{Tyr}$ and may be involved in the specific recognition of the anticodon [4]; and (3) the C-terminal domain (C-TyrRS, residues 321–419), which shows a very low electron density that hampers the tracing of its polypeptide chain. Experiments with truncated homo- and heterodimers lacking the C-terminal domain have shown that C-TyrRS is necessary for $tRNA^{Tyr}$ binding and charging and that one $tRNA^{Tyr}$ molecule binds to the C-terminal domain of one monomer and to the N-terminal α/β domain of the other monomer [5, 6]. Site-directed mutagenesis experiments have identified six basic residues (R_{368}, R_{371}, R_{407}, R_{408}, K_{410}, and K_{411}) that are necessary for $tRNA^{Tyr}$ charging [7]. The recombinant protein TyrRS(Δ4) contains residues 320–419 and a Leu-Glu-His_6 C-terminal extension. It therefore corresponds to an isolated C-TyrRS domain. TyrRS(Δ4) behaves as a folded globular monomeric protein in solution, and circular dichroism experiments have indicated that its structure is effectively identical to that of C-TyrRS in the context of the full-length synthetase [8–10]. The secondary structure of TyrRS(Δ4) is novel among the anticodon arm binding domains of synthetases [9]. Here, we report the three-dimensional solution structure of TyrRS(Δ4) and its backbone dynamics, determined by nuclear magnetic resonance (NMR).

Results and Discussion

Structure Description

The structure of TyrRS(Δ4) is composed of a five-stranded β sheet, flanked on one side by two α helices that run roughly antiparallel to one another and on the other side by a third α helix (Figure 1; Table 1).

The nine N-terminal residues of TyrRS(Δ4) are disordered, especially the first five residues, which showed no nOes with the rest of the protein or whose amide NMR signals were not observed. The first α helix (α_1: 332–339) is connected by a hairpin loop to a β strand (β_1: 344–347). A less well-defined loop, centered at residue 349, leads to two antiparallel α helices (α_2: 354–361 and α_3: 367–375) that are followed by four strands of the β sheet (β_2: 379–381, β_3: 384–385, β_4: 404–408, and β_5: 413–418). Strands β_2 and β_3 are linked by a short two-residue turn, while strands β_3 and β_4 are connected by a long, meander-shaped loop (386–403) with a short helical segment (α_4: 395–397) in the middle. Except for

[4] Correspondence: murield@pasteur.fr (M.D.), hbedouel@pasteur.fr (H.B.)
[5] These authors contributed equally to this work.
[6] Present address: International Centre for Genetic Engineering and Biotechnology, Area Science Park, Padriciano 99, 34012 Trieste, Italy.

Key words: anticodon arm binding domain; aminoacyl-tRNA synthetase; *Bacillus stearothermophilus*; NMR; ^{15}N relaxation; translation

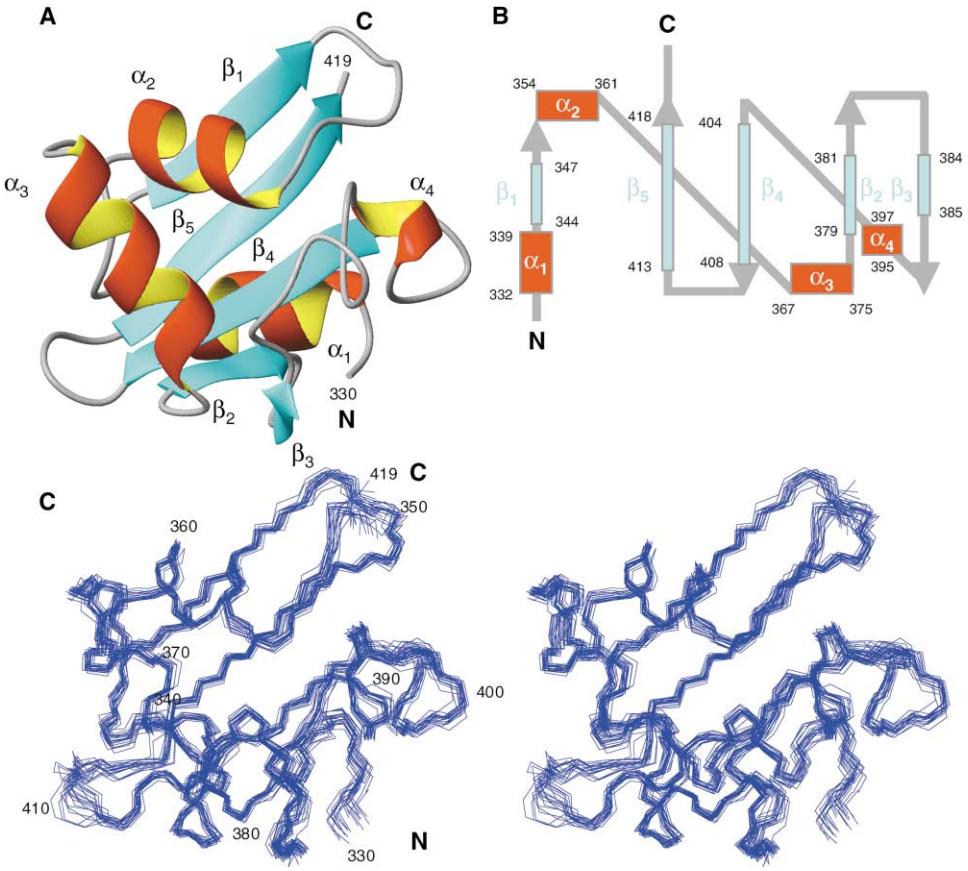

Figure 1. Structure of TyrRS(Δ4)

(A) Ribbon drawing of one conformer chosen to represent the structural ensemble. N and C; N and C terminus, respectively. The disordered N-terminal residues are not shown.

(B) Secondary structure topology. Helices are shown in red and β strands in cyan as in (A). Numbers indicate their starting and ending residues. The size of a rectangle does not accurately represent the relative length of the corresponding secondary structure element.

(C) Stereo view of the backbone superposition of the 20-conformer structural ensemble.

β_1, which runs parallel to β_5, the arrangement of the sheet strands is antiparallel.

Helix α_1 and the β sheet are packed against each other through hydrophobic interactions that involve A_{332}, I_{335}, and F_{339} in helix α_1 and V_{405}, Y_{413}, Y_{414}, and L_{415} in strands β_4 and β_5. Residues L_{330}, V_{342}, N_{382}, and F_{403} also make important contributions to the packing interactions on this side of the sheet. The main hydrophobic core of the protein is essentially formed by the packing of helix α_2, helix α_3, and the other side of the β sheet (strands β_2, β_4, and β_5). The hydrophobic residues belonging to secondary structure elements and contributing to this core include L_{354}, L_{357}, L_{358}, and V_{355} from helix α_2, A_{370} and I_{374} from helix α_3, I_{379} and V_{381} from strand β_2, and I_{406} and I_{416} from strands β_4 and β_5, respectively. Residues I_{363}, I_{392}, and A_{395}, located in loop regions, also participate in this core. Finally, helices α_2 and α_3 are held together mainly by hydrophobic interactions between L_{354}, V_{355}, L_{358}, V_{359}, A_{370}, and I_{374}.

Correlating the Backbone Dynamics and the Structure

The N and C termini of TyrRS(Δ4) show low values of the order parameter S^2, which indicate high amplitude motions on the ps-ns time scale (Figure 2). In contrast, the rest of the protein displays high S^2 values (except for residues G_{349} and G_{350} in loop β_1-α_2), typical of globular proteins. All residues within the helices and β sheet have S^2 values ca. ≥ 0.80, while some residues in loops show slightly lower values. The S^2 and backbone rmsd values of the structural ensemble are inversely correlated for the N and C termini as well as for loop β_1-α_2. These correlations indicate that internal motions on the ps-ns time scale are responsible for the structural variability observed in these regions. Loop β_4-β_5 has high rmsd values that could also be due to the dynamics of the protein. Indeed, no amide NMR signals were detected for K_{410} and K_{411}, probably because of exchange broadening. The remaining regions showing rmsd values significantly higher than the mean are centered at residues E_{341}, G_{383}, G_{390}, E_{396}, and E_{400}. These residues have high S^2 values. Such values indicate the absence of fast motions of high amplitude and suggest that the higher rmsd values are due to the reduced number of experimental restraints in these solvent-exposed loop regions. Finally, high R_{ex} rates, indicative of slow local conformational exchange on the μs-ms time scale, are observed in helices α_1 and α_3 as well as in loop regions.

Table 1. Statistics of the NMR Structural Ensemble of TyrRS(Δ4)

Parameter	Value
DYANA	
Number of nOe upper distance limits[a]	1352
Number of dihedral angle constraints	71
Number of hydrogen bonds	33
Residual target function (Å^2; mean value for 50 conformers)	5.72 ± 0.66
OPAL (average for the best 20 conformers)	
Residual distance constraint violations	
Number ≥ 0.1 Å	3.90 ± 2.12
Maximum (Å)	0.10 ± 0.01
Residual dihedral angle constraint violations	
Number ≥ 2.0°	0.55 ± 0.59
Maximum (°)	2.01 ± 0.24
AMBER energies (kcal/mol)	
Total	−3,974 ± 54
Van der Waals	−247 ± 10
Electrostatic	−4,645 ± 66
Mean pairwise rmsd (Å)[b]	
Backbone atoms N, Cα, and C′ (330–418)	0.57 ± 0.09
Heavy atoms (330–418)	1.38 ± 0.19
Ensemble Ramachandran plot	
Residues in most favoured regions	68.6%
Residues in additional allowed regions	29.3%
Residues in generously allowed regions	1.8%
Residues in disallowed regions	0.4%

[a] Unambiguous meaningful nOes used for structure calculations (389 long range, 297 medium range, 372 sequential, and 294 intraresidue nOes).

[b] Mean of the pairwise rmsd between residues 330 and 418, thus excluding the flexible N and C termini.

Possible Cause of the Crystallographic Disorder of C-TyrRS

The disorder observed for C-TyrRS in the crystals of the full-length protein [3] could be of either static origin (same structure of C-TyrRS at different positions within the lattice) or dynamic origin (high mobility within the domain). ^{15}N relaxation data show that the N-terminal residues of TyrRS(Δ4) are disordered and highly mobile while the rest of the molecule displays typical dynamics of a well-ordered and structured globular protein. These observations suggest that the disorder observed in the crystals is of static origin and that it is due to the flexibility of the peptide linking the α-helical and C-terminal domains. In the context of the full-length protein, interactions of the linker and/or C-TyrRS with the rest of the protein could restrict its mobility. Available data, however, do not support this latter possibility. Indeed, (1) the N- and C-terminal fragments (residues 1–317 and 321–419, respectively) can fold independently into entities that are stable under conditions similar to those used for crystallization; (2) the structures of the α/β- and α-helical domains are identical in the crystals of either the full-length protein or the N-terminal fragment [3, 11]; (3) the structure of the C-terminal domain is effectively the same whether this domain is isolated in solution [TyrRS(Δ4)] or present in the context of the full-length TyrRS, as revealed by circular dichroism in the far and near UV regions [10]; (4) double hybrid experiments failed to show any interaction between the C- and N-terminal fragments [12]; and (5) several TyrRS insertion mutations, containing up to five residues in the linker region (position 325), had no significant effect on its specific activity [4]. As these insertions were rich in glycines, this result indicates that the linker can be flexible (and of variable length) without compromising the aminoacylation activity of TyrRS. Taken together, these arguments strongly suggest that the linker region is flexible in TyrRS and that the C-terminal domain does not interact strongly with the remainder of the protein. TyrRS would thus be the only aminoacyl synthetase that has not evolved strong interactions between its anticodon arm binding domain and its catalytic domain.

Structural Similarity between TyrRS(Δ4) and Other RNA Binding Proteins

Sequence alignments have predicted that the C-terminal domains of eubacterial tyrosyl-tRNA synthetases contain the so-called "S4 motif," which is also present in the proteins of several families with diverse functions [13–15]. The role of this motif would be to display positively charged residues for interaction with the phosphates of an RNA ligand [15]. Accordingly, when the coordinates of the TyrRS(Δ4) structure were submitted to the server DALI [16], three structures containing the S4 motif showed significant homologies with TyrRS(Δ4) (statistical Z score > 2.0). These were: the *Escherichia coli* ribosome binding heat shock protein Hsp15 ($Z = 4.5$), the ETS domain of *B. stearothermophilus* ribosomal protein S4 ($Z = 4.7$), and, to a lesser extent, the N-terminal domain N1 of the *E. coli* threonyl-tRNA synthetase (ThrRS, $Z = 2.4$), whose function is unknown [13, 15, 17]. Despite low sequence identity (≤20% relative to C-TyrRS), the above domains display a common fold, consisting of a three- or four-stranded antiparallel β sheet packed against two α helices (Figure 3). A comparison of the structures of Hsp15, S4, and ThrRS has previously revealed a structurally similar region between α_2 and β_4 [TyrRS(Δ4) numbering], the αL motif [15]. Most

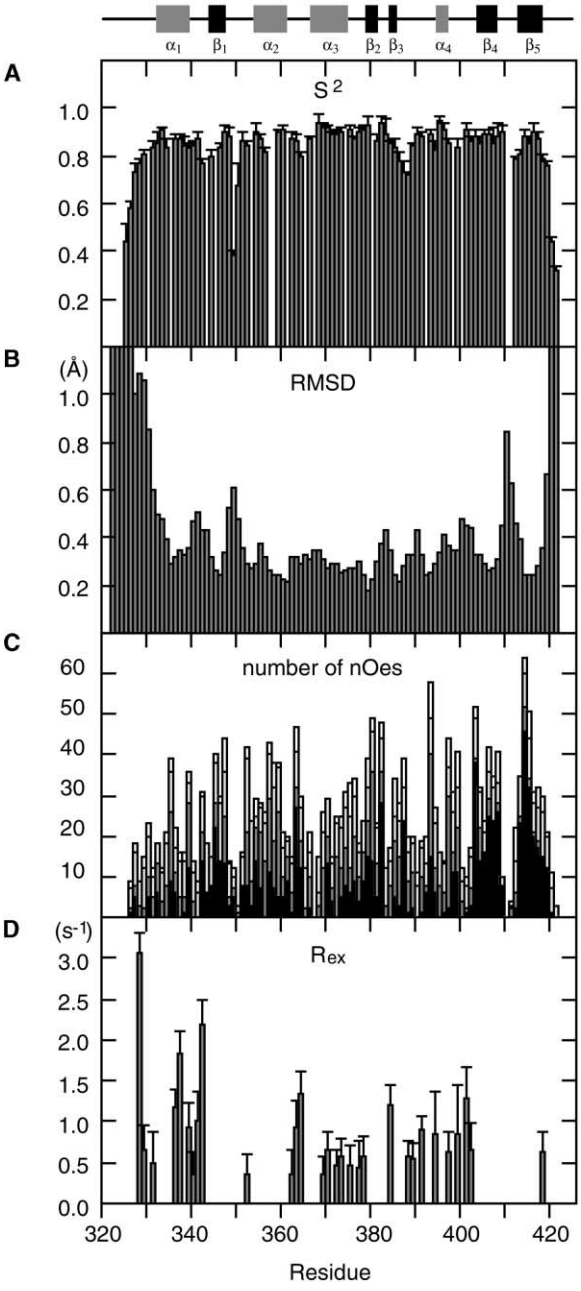

Figure 2. TyrRS(Δ4) Backbone Dynamics, Rmsd of the Calculated Structural Ensemble, and the nOes Used for Obtaining the Structures

(A) Order parameter (S^2). S^2 reflects the amplitude of fast internal motions of the NH vector in the ps-ns time scale and varies between 0 (high-amplitude motions) and 1 (rigid body).

(B) Backbone (C′, N, and Cα) rmsd from the mean structure after best superposition of each structure to the mean structure between residues 330 and 418.

(C) Number of meaningful nOes between residues i and j used as constraints in structure calculations: white, intraresidue (j = i); light gray, sequential (j = i +1); dark gray, medium range (i + 2 ≤ j ≤ i + 4); black, long range (j ≥ i + 5).

(D) Rate of conformational exchange (R_{ex}, in s^{-1}) that indicates slow conformational exchange on the μs-ms time scale. S^2 and R_{ex} values were obtained using an isotropic rotational correlation time of 6.85 ns. Error bars are displayed for these parameters.

of the residues conserved across the families are in the α_2–α_3 and β_2–β_3 regions, and some of these are exposed to the solvent. The buried residues involved in packing helices α_2 and α_3 together are particularly similar in the four proteins. The main structural differences between TyrRS(Δ4) and the other proteins are located in the long β_3-β_4 loop. The length of this loop in TyrRS(Δ4) and its low sequence similarity may explain these differences.

Comparison with Other Eubacterial TyrRS C-Terminal Domains

The sequences of 27 C-TyrRS domains from eubacteria were retrieved and aligned as described in [4]. The main features of this alignment are summarized on the sequence of *B. stearothermophilus* C-TyrRS in Figure 3E. The conserved residues mainly belong to the region between α_2 and β_3, which is included in the S4 motif, and to the region between β_4 and β_5, rich in basic residues. All the hydrophobic residues that contribute to the main core of C-TyrRS (see above) are conserved, except I_{392} and A_{395} in the long β_3-β_4 loop. In particular, all the buried residues involved in interactions between helices α_2 and α_3 are conserved (≥50% identity), and these are also very similar in the other RNA binding protein families. Therefore, the interactions that contribute to the packing of helices α_2 and α_3 together and against one side of the sheet appear important to preserve the S4 motif, while the β_3-β_4 loop seems less important. The conservation of hydrophobic residues also suggests that the S4 motif is preserved among the eubacterial TyrRSs. In contrast, several residues involved in packing the protein on the other side of the sheet are not conserved. Finally, only L_{322}, L_{330}, and I_{335} are conserved between residues 321 and 340, together with the functionally essential residue F_{323} [4].

tRNA Binding

In vitro tRNA charging and in vivo complementation experiments have shown that six basic residues of the C-terminal domain are important for the interaction of TyrRS with $tRNA^{Tyr}$ [7]. These residues are highly exposed to the solvent, except for the nonconserved residue R_{408}, which is less exposed. The six residues lie on the same face of the molecule and constitute a highly positive surface that can bind the negatively charged tRNA (Figures 4A and 4B). They are located in two separate regions. The first one involves R_{368} and R_{371}, the latter residue being conserved across the four families of RNA binding proteins. Interestingly, S4 and Hsp15 show conserved residues within a positively charged patch in an equivalent spatial region. In the case of S4, this region contacts the 16S ribosomal RNA [18]. Residues R_{407}, R_{408}, K_{410}, and K_{411}, located in strand β_4 and loop β_4-β_5, constitute the second positive region, which is conserved among the TyrRSs but has no equivalent in S4 or Hsp15. This suggests that, in TyrRS, the general S4 motif is complemented by an idiosyncratic motif to specifically recognize $tRNA^{Tyr}$. Five other basic residues have been mutated in the C-terminal domain of TyrRS and found to be irrelevant for in vivo $tRNA^{Tyr}$ charging in complementation experiments [7]. Three of these, R_{402}, R_{417}, and R_{398}, lie on the opposite face of the

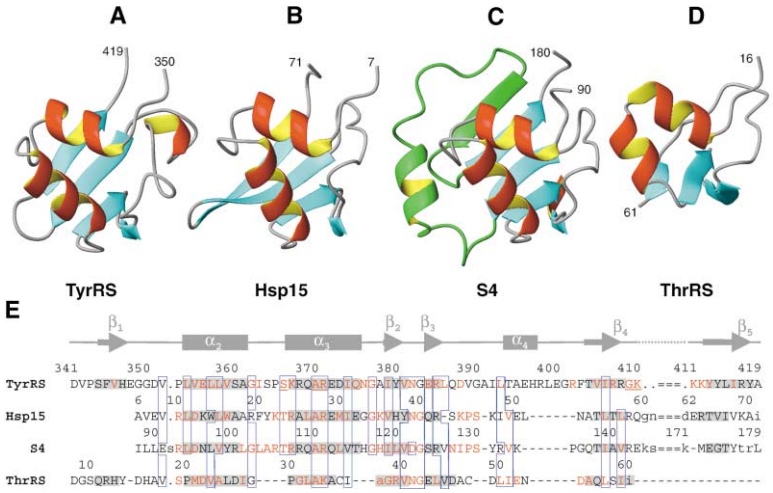

Figure 3. Comparison of TyrRS(Δ4) with Other RNA Binding Proteins

(A–D) Ribbon diagram of the structure of (A) TyrRS(Δ4), (B) Hsp15 (Z score = 4.5, Cα rmsd = 2.2 Å over 62 residues), (C) S4 (Z score = 4.7, Cα rmsd = 2.1 Å over 60 residues), and (D) the N1 domain of ThrRS (Z score = 2.4, Cα rmsd = 2.5 Å over 59 residues). Only the regions with structural homology are shown. The region 144–171 of S4 that is absent in the other proteins is shown in green.

(E) Sequence alignment based on structure superposition obtained from the server DALI [16]. The secondary structure of TyrRS(Δ4) is represented on top of the alignment and the sequences of corresponding secondary structure elements, as determined by MOLMOL [39], are shaded in gray. Residues 146–170 of S4 are not represented. The short β strands 11–13 and 55–56 of ThrRS belong to another β sheet and should not be taken as part of the S4 module. These strands are not represented in (D). Residues in lower case were not considered to obtain the alignment. Structurally similar conserved or identical (≥50%) residues within each family are colored in red. The highly conserved (≥85% identical) residues of TyrRS are underlined. Residues that are similar or identical in at least three of the proteins are boxed. Residue conservation information for Hsp15, S4, and ThrRS is taken from [15].

molecule, indicating that only one face of the molecule is implicated in the interaction with $tRNA^{Tyr}$ (Figure 4C). These residues form two positive patches in an otherwise rather negative surface. The other residues, K_{367} and R_{385}, are on two edges of the binding face. Several residues for which no experimental data are available are exposed on the face of C-TyrRS that interacts with $tRNA^{Tyr}$ (Figure 4D). Some are conserved among eubacteria and could participate in tRNA binding through ionic interactions, hydrogen bonds, or aromatic ring stacking with bases S_{366}, Q_{375}, N_{376}, G_{377}, G_{409}, K_{412}, and Y_{413}. Interestingly, mutation S_{356} → A in *Acidobacillus ferrooxidans* TyrRS (S_{356} is equivalent to S_{366} in *B. stearothermophilus*) increases significantly its K_M for $tRNA^{Tyr}$ [19]. Mutagenesis experiments of these residues and/or the structure of the complex of TyrRS with its cognate tRNA should

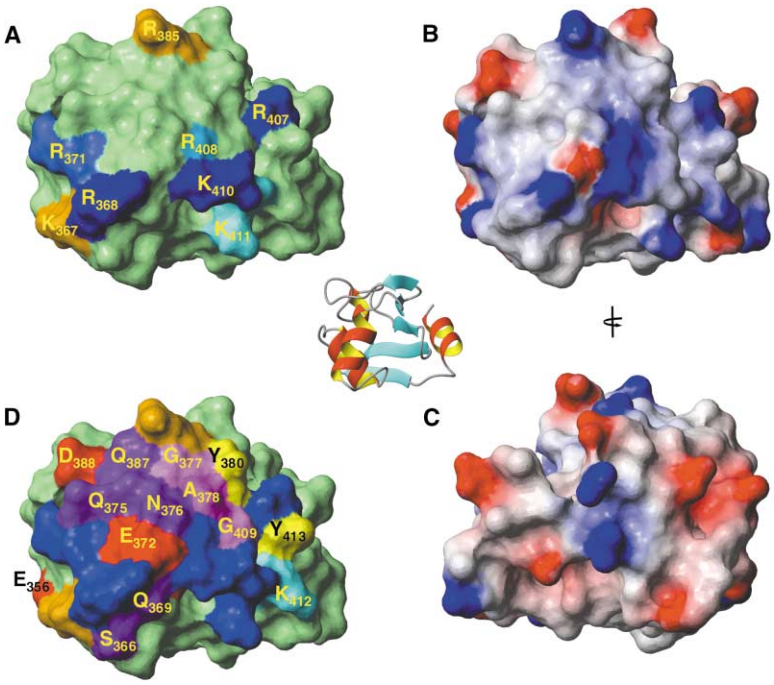

Figure 4. Surface Representations of the Structure of TyrRS(Δ4)

Residues 330–418. A ribbon diagram is displayed at the center of the figure to show the orientation of the molecule used in the surface representations.

(A) The six basic residues identified by mutagenesis as essential for interaction with $tRNA^{Tyr}$ are shown in blue, while mutated residues that are not relevant to tRNA interaction as assessed by an in vivo genetic complementation assay [7] are represented in orange. Different blues are used for clarity.

(B and C) Surface electrostatic potential of TyrRS(Δ4) in the same orientation as in (A) and after a 180° y rotation, respectively. Positive and negative potentials are represented in blue and red, respectively. Electrostatic potentials were calculated with MOLMOL [39].

(D) Analysis of the putative binding surface. The basic residues known to be important (blue) or irrelevant for tRNA binding (orange) shown in (A) are displayed without label. The remaining residues on the tRNA binding face are labeled and colored: red, negatively charged residues that most probably do not interact with tRNA; cyan, positively charged residues that could in principle interact with tRNA phosphates; dark purple and violet, polar residues (purple) and glycines (violet) with an exposed amide group that could form hydrogen bonds with tRNA bases or ribose; yellow, exposed aromatic residues that could stack with tRNA bases; purple, A_{378}.

help in establishing the relevance of these residues for the interaction.

Biological Implications

The C-terminal domain of TyrRS, which interacts with the anticodon arm of $tRNA^{Tyr}$, is essential for binding and charging $tRNA^{Tyr}$. The structure of TyrRS(Δ4) presented here is the first described for the C-terminal domain of a tyrosyl-tRNA synthetase and shows a novel fold among the anticodon arm binding domains of aminoacyl-tRNA synthetases. The structure contains the S4 motif, which is also present in other families of RNA binding proteins. The conservation profile of residues involved in maintaining the architecture of TyrRS(Δ4) indicates that this structure represents a prototype for the C-terminal domain of the eubacterial TyrRSs. TyrRS(Δ4) displays a face rich in positive residues, which interacts with the negatively charged tRNA. Six of these residues have, indeed, previously been shown by mutagenesis to be important for $tRNA^{Tyr}$ binding. The other evolutionary conserved residues on this face may interact with phosphate, ribose, or base moieties of $tRNA^{Tyr}$. The structure thus allows one to rationalise previous mutagenesis data and to pinpoint further mutagenesis sites. The conservation of solvent-exposed residues on the binding face of TyrRS(Δ4) suggests that the C-terminal domain of the other eubacterial TyrRSs bind their cognate $tRNA^{Tyr}$ by similar mechanisms.

The structure of TyrRS(Δ4) completes that of the free enzyme from *B. stearothermophilus* for which only the structure of the N-terminal region could be solved by X-ray crystallography [3]. Whenever the structure of a complex between TyrRS and $tRNA^{Tyr}$ is available, it will be possible to compare the structures of the free and bound C-terminal domain and thereby establish whether conformational changes are involved in the interaction.

Experimental Procedures

Sample Preparation

^{15}N- and ^{15}N, ^{13}C-labeled recombinant TyrRS(Δ4) was expressed in *E. coli* and purified as described [9]. Samples were prepared in 20 mM potassium phosphate buffer (pH 6.8) with a protein concentration ranging from 0.8 to 1.2 mM.

NMR

NMR experiments were run at 35°C on a Varian Inova spectrometer resonating at a 499.83 MHz ^1H frequency. Vnmr (Varian) and XEASY [20] were used for data processing and analysis. ^1H, ^{15}N, and ^{13}C sequential assignments were achieved using a combination of triple resonance CBCA(CO)NH and HNCACB experiments [21] and of three-dimensional ^{15}N-edited NOESY-HSQC and TOCSY-HSQC spectra [22]. ^1H and ^{13}C side chain assignments were performed using 3D H(CC-TOCSY)NNH, C(CC-TOCSY)NNH [23, 24], 3D ^{13}C-edited HCCH-TOCSY [25], ^{15}N-edited TOCSY-HSQC [22], 2D ^1H-^1H DQF-COSY [26, 27], and 2D experiments to correlate aromatic protons with C_β carbons [28].

Distance constraints were derived from a 3D ^{15}N-edited NOESY-HSQC spectrum recorded in H_2O with a 150 ms mixing time as well as from a 2D ^1H-^1H NOESY spectrum acquired in D_2O with a mixing time of 100 ms. The latter NOESY was acquired on an 800 MHz Bruker DRX-800 spectrometer. nOe intensities were evaluated from peak heights and calibrated using the CALIBA routine of DYANA [29]. $J_{HNH\alpha}$ coupling constraints were obtained from an HMQC-J [30] spectrum as described [9] and converted to constraints for ϕ dihedral angles as follows: ($-90°$, $-40°$) for $J_{HNH\alpha} < 5.5$ Hz and ($-160°$, $-80°$) for $J_{HNH\alpha} > 8$ Hz.

^{15}N Relaxation Measurements and Analysis

Longitudinal (R_1) and transverse (R_2) ^{15}N amide relaxation rates as well as ^{15}N-^1H nOe data were obtained with pulse schemes described by Kay and coworkers [31]. Nine relaxation-time data points were used to determine R_1 (60–1000 ms) and R_2 (10–190 ms). R_1 and R_2 data were fitted to monoexponential decays without offset. Error on data points was estimated as 4 (R_1 and R_2) or 3 (nOe) noise rmsds. Relaxation data were analyzed using the extended [32] Lipari and Szabo formalism [33] with MODELFREE version 4.1 [34, 35]. The statistical approach to model selection [35] was followed. Isotropic tumbling was assumed as the ratio of the parallel and perpendicular axes of the diffusion tensor [36] was very close to unity (1.080 ± 0.008).

nOe Assignments and Structure Calculations

Starting from 639 manually assigned peaks (mostly intraresidual, sequential, and secondary structure-related nOes), a total number of 2017 nOe peaks from the ^{15}N-edited NOESY-HSQC (H_2O) and from the 2D NOESY (D_2O) spectra were assigned using 48 cycles of simulated annealing within NOAH [37]. nOe assignments were carefully inspected and completed manually. This procedure resulted in 1352 meaningful upper distance constraints. Experimental constraints also included 71 ϕ dihedral angles and 33 backbone-backbone hydrogen bonds. A hydrogen bond constraint was added only when 67% of the preliminary structures showed a hydrogen bond, and this was in agreement with saturation transfer [9] and hydrogen exchange in D_2O experiments.

From the 150 structures calculated using the torsion angle dynamics protocol in DYANA [29], the 50 structures with the lowest target function value were subjected to restrained energy minimization in water using OPAL [38] with the AMBER94 force field. The 20 structures with the lowest total energy values were selected as representative of the TyrRS(Δ4) structure (Table 1). Structures were displayed and analyzed with MOLMOL [39]; their quality was evaluated using PROCHECK [40].

Supplementary Material

A supplemental table showing relaxation (R_1, R_2, and nOe) and "model-free" (order parameters, R_{ex}, and internal correlation time) parameters can be found at http://images.cellpress.com/supmat/supmatin.htm.

Acknowledgments

We thank C. Simenel and C. Castagné for assistance with NMR experiments, E. Guittet for time on a Bruker 800 MHz spectrometer, and Shamila Nair for critical reading of the manuscript.

Received: August 31, 2001
Revised: December 13, 2001
Accepted: December 17, 2001

References

1. Cusack, S. (1997). Aminoacyl-tRNA synthetases. Curr. Opin. Struct. Biol. *7*, 881–889.
2. Wolf, Y.I., Aravind, L., Grishin, N.V., and Koonin, E.V. (1999). Evolution of aminoacyl-tRNA synthetases—analysis of unique domain architectures and phylogenetic trees reveals a complex history of horizontal gene transfer events. Genome Res. *9*, 689–710.
3. Brick, P., Bhat, T.N., and Blow, D.M. (1989). Structure of tyrosyl-tRNA synthetase refined at 2.3 Å resolution. Interaction of the enzyme with the tyrosyl adenylate intermediate. J. Mol. Biol. *208*, 83–98.
4. Gaillard, C., and Bedouelle, H. (2001). An essential residue in the flexible peptide linking the two idiosynchratic domains of bacterial tyrosyl-tRNA synthetases. Biochemistry *40*, 7192–7199.
5. Waye, M.M., Winter, G., Wilkinson, A.J., and Fersht, A.R. (1983). Deletion mutagenesis using an 'M13 splint': the N-terminal structural domain of tyrosyl-tRNA synthetase (*B. stearother-*

mophilus) catalyses the formation of tyrosyl adenylate. EMBO J. *2*, 1827–1829.
6. Carter, P., Bedouelle, H., and Winter, G. (1986). Construction of heterodimer tyrosyl-tRNA synthetase shows $tRNA^{Tyr}$ interacts with both subunits. Proc. Natl. Acad. Sci. USA *83*, 1189–1192.
7. Bedouelle, H., and Winter, G. (1986). A model of synthetase/transfer RNA interaction as deduced by protein engineering. Nature *320*, 371–373.
8. Guez-Ivanier, V., and Bedouelle, H. (1996). Disordered C-terminal domain of tyrosyl transfer-RNA synthetase: evidence for a folded state. J. Mol. Biol. *255*, 110–120.
9. Pintar, A., Guez, V., Castagné, C., Bedouelle, H., and Delepierre, M. (1999). Secondary structure of the C-terminal domain of the tyrosyl-transfer RNA synthetase from *Bacillus stearothermophilus*: a novel type of anticodon binding domain? FEBS Lett. *446*, 81–85.
10. Guez, V., Nair, S., Chaffotte, A., and Bedouelle, H. (2000). The anticodon-binding domain of tyrosyl-tRNA synthetase: state of folding and origin of the crystallographic disorder. Biochemistry *39*, 1739–1747.
11. Brick, P., and Blow, D.M. (1987). Crystal structure of a deletion mutant of a tyrosyl-tRNA synthetase complexed with tyrosine. J. Mol. Biol. *194*, 287–297.
12. Karimova, G., Ullmann, A., and Ladant, D. (2001). Protein-protein interaction between *Bacillus stearothermophilus* tyrosyl-tRNA synthetase subdomains revealed by a bacterial two-hybrid system. J. Mol. Microbiol. Biotechnol. *3*, 73–82.
13. Markus, M.A., Gerstner, R.B., Draper, D.E., and Torchia, D.A. (1998). The solution structure of ribosomal protein S4 Δ41 reveals two subdomains and a positively charged surface that may interact with RNA. EMBO J. *17*, 4559–4571.
14. Aravind, L., and Koonin, E.V. (1999). Novel predicted RNA-binding domains associated with the translation machinery. J. Mol. Evol. *48*, 291–302.
15. Staker, B.L., Korber, P., Bardwell, J.C., and Saper, M.A. (2000). Structure of Hsp15 reveals a novel RNA-binding motif. EMBO J. *19*, 749–757.
16. Holm, L., and Sander, C. (1993). Protein structure comparison by alignment of distances matrices. J. Mol. Biol. *233*, 123–138.
17. Sankaranarayanan, R., Dock-Bregeon, A.C., Romby, P., Caillet, J., Springer, M., Rees, B., Ehresmann, C., Ehresmann, B., and Moras, D. (1999). The structure of threonyl-tRNA synthetase-$tRNA^{Thr}$ complex enlightens its repressor activity and reveals an essential zinc ion in the active site. Cell *97*, 371–381.
18. Wimberly, B.T., Brodersen, D.E., Clemons, W.M., Jr., Morgan-Warren, R.J., Carter, A.P., Vonrhein, C., Hartsch, T., and Ramakrishnan, V. (2000). Structure of the 30S ribosomal subunit. Nature *407*, 327–339.
19. Salazar, J.C., Zuñiga, R., Lefimil, C., Söll, D., and Orellana, O. (2001). Conserved amino acids near the carboxy terminus of bacterial tyrosyl-tRNA synthetase are involved in tRNA and Tyr-AMP binding. FEBS Lett. *491*, 257–260.
20. Bartels, C., Xia, T.-H., Billeter, M., Güntert, P., and Wüthrich, K. (1995). The program XEASY for computer-supported NMR spectral analysis of biological macromolecules. J. Biomol. NMR *6*, 1–10.
21. Muhandiram, D.R., and Kay, L.E. (1994). Gradient-enhanced triple-resonance three-dimensional NMR experiments with improved sensitivity. J. Magn. Reson. B *103*, 203–216.
22. Zhang, O., Kay, L.E., Olivier, J.P., and Forman-Kay, D. (1994). Backbone ^1H and ^{15}N resonance assignments of the N-terminal SH3 domain of drk in folded and unfolded states using enhanced-sensitivity pulsed field gradient NMR techniques. J. Biomol. NMR *4*, 845–858.
23. Grzesiek, S., Anglister, J., and Bax, A. (1993). Correlation of backbone amide and aliphatic side-chain resonances in $^{13}C/^{15}N$-enriched proteins by isotropic mixing of ^{13}C magnetization. J. Magn. Reson. B *101*, 114–119.
24. Logan, T.M., Olejniczak, E.T., Xu, R.X., and Fesik, S.W. (1993). A general method for assigning NMR spectra of denatured proteins using 3D HC(CO)NH-TOCSY triple resonance experiments. J. Biomol. NMR *3*, 225–231.
25. Kay, L.E., Xu, G., Singer, A.U., Muhandiram, D.R., and Forman-Kay, J.D. (1993). A gradient-enhanced HCCH-TOCSY experiment for recording side-chain ^1H and ^{13}C correlations in H_2O samples of proteins. J. Magn. Reson. B *101*, 333–337.
26. Piantini, U., Sørensen, O.W., and Ernst, R.R. (1982). Multiple quantum filters for elucidating NMR coupling networks. J. Am. Chem. Soc. *104*, 6800–6801.
27. Rance, M., Sorensen, O.W., Bodenhausen, G., Wagner, G., Ernst, R.R., and Wuthrich, K. (1983). Improved spectral resolution in cosy ^1H NMR spectra of proteins via double quantum filtering. Biochem. Biophys. Res. Comm. *117*, 479–485.
28. Yamazaki, T., Forman-Kay, J.D., and Kay, L.E. (1993). Two-dimensional NMR experiments for correlating $^{13}C\beta$ and $^1H\delta/\epsilon$ chemical shifts of aromatic residues in ^{13}C-labeled proteins via scalar couplings. J. Am. Chem. Soc. *115*, 11054–11055.
29. Güntert, P., Mumenthaler, C., and Wüthrich, K. (1997). Torsion angle dynamics for NMR structure calculation with the new program DYANA. J. Mol. Biol. *273*, 283–298.
30. Kay, L.E., and Bax, A. (1990). New methods for the measurement of NH-$C\alpha$H coupling constants in ^{15}N-labeled proteins. J. Magn. Reson. *86*, 110–126.
31. Farrow, N.A., Muhandiram, R., Singer, A.U., Pascal, S.M., Kay, C.M., Gish, G., Shoelson, S.E., Pawson, T., Forman-Kay, J.D., and Kay, L.E. (1994). Backbone dynamics of a free and phosphopeptide-complexed Src homology 2 domain studied by ^{15}N NMR relaxation. Biochemistry *33*, 5984–6003.
32. Clore, G.M., Szabo, A., Bax, A., Kay, L.E., Driscoll, P.C., Gronenborn, A.M. (1990). Deviations from the simple two-parameter model-free approach to the interpretation of nitrogen-15 nuclear magnetic relaxation of proteins. J. Am. Chem. Soc. *112*, 4989–4991.
33. Lipari, G., and Szabo, A. (1982). Model-free approach to the interpretation of nuclear magnetic resonance relaxation in macromolecules. J. Am. Chem. Soc. *104*, 4559–4570.
34. Palmer, A.G., Rance, M., and Wright, P.E. (1991). Intramolecular motions of a zinc finger DNA-binding domain from Xfin characterized by proton-detected natural abundance ^{13}C heteronuclear NMR spectroscopy. J. Am. Chem. Soc. *113*, 4371–4380.
35. Mandel, A.M., Akke, M., and Palmer, A.G. (1995). Backbone dynamics of *Escherichia coli* ribonuclease HI: correlations with structure and function in an active enzyme. J. Mol. Biol. *246*, 144–163.
36. Tjandra, N., and Bax, A. (1995). Rotational diffusion anisotropy of human ubiquitin from ^{15}N NMR relaxation. J. Am. Chem. Soc. *117*, 12562–12566.
37. Mumenthaler, C., Güntert, P., Braun, W., and Wüthrich, K. (1997). Automated combined assignment of NOESY spectra and three-dimensional protein structure determination. J. Biomol. NMR *10*, 351–362.
38. Luginbühl, P., Güntert, P., Billeter, M., and Wüthrich, K. (1996). The new program OPAL for molecular dynamics simulations and energy refinements of biological macromolecules. J. Biomol. NMR *8*, 136–146.
39. Koradi, R., Billeter, M., and Wüthrich, K. (1996). MOLMOL: a program for display and analysis of macromolecular structures. J. Mol. Graph. *14*, 51–55.
40. Laskowski, R.A., MacArthur, M.W., Moss, D.S., and Thornton, J.M. (1993). PROCHECK: a program to check the stereochemical quality of protein structures. J. Appl. Crystallogr. *26*, 283–291.

Accession Numbers

The atomic coordinates of the structure of TyrRS(Δ4) have been deposited in the RCBS Protein Data Bank (code 1JH3); chemical shift data have been deposited in the BioMagResBank (accession code 5070).